Projected Changes in Mean and Extreme Precipitation in Africa under Global Warming. Part II: East Africa

MXOLISI E. SHONGWE,* GEERT JAN VAN OLDENBORGH, AND BART VAN DEN HURK

Royal Netherlands Meteorological Institute, De Bilt, Netherlands

MAARTEN VAN AALST

Red Cross/Red Crescent Climate Centre, The Hague, Netherlands

(Manuscript received 7 October 2008, in final form 23 November 2010)

ABSTRACT

Probable changes in mean and extreme precipitation in East Africa are estimated from general circulation models (GCMs) prepared for the Intergovernmental Panel on Climate Change Fourth Assessment Report (AR4). Bayesian statistics are used to derive the relative weights assigned to each member in the multimodel ensemble. There is substantial evidence in support of a positive shift of the whole rainfall distribution in East Africa during the wet seasons. The models give indications for an increase in mean precipitation rates and intensity of high rainfall events but for less severe droughts. Upward precipitation trends are projected from early this (twenty first) century. As in the observations, a statistically significant link between sea surface temperature gradients in the tropical Indian Ocean and short rains (October–December) in East Africa is simulated in the GCMs. Furthermore, most models project a differential warming of the Indian Ocean during boreal autumn. This is favorable for an increase in the probability of positive Indian Ocean zonal mode events, which have been associated with anomalously strong short rains in East Africa. On top of the general increase in rainfall in the tropics due to thermodynamic effects, a change in the structure of the Eastern Hemisphere Walker circulation is consistent with an increase in East Africa precipitation relative to other regions within the same latitudinal belt. A notable feature of this change is a weakening of the climatological subsidence over eastern Kenya. East Africa is shown to be a region in which a coherent projection of future precipitation change can be made, supported by physical arguments. Although the rate of change is still uncertain, almost all results point to a wetter climate with more intense wet seasons and less severe droughts.

1. Introduction

The chemical composition of the atmosphere is changing owing to human activities, triggering numerous studies aimed at understanding the sensitivity of the climate system to rising greenhouse gas concentrations (Houghton et al. 2001; Solomon et al. 2007, and references therein). Although the increase in greenhouse gases is relatively uniform around the globe, the response in a myriad of climate variables inevitably exhibits spatial inhomogeneities. For this reason, many studies have focused on possible impacts of climate change on selected climate variables in specific regions of the globe, especially those variables considered economically and socially significant (e.g., Gillett et al. 2004a; Karoly and Braganza 2005; Hegerl et al. 2006; van Ulden and van Oldenborgh 2006; van den Hurk et al. 2006; Beniston et al. 2007).

Considerable effort has been devoted to investigating possible changes in mean climate, and increasingly also to changes in variability and extremes, in the Northern Hemisphere continental areas. This is related to the availability of expertise and reliable data in these areas. By comparison, many of the least developed countries, especially in Africa, suffer from both a lack of high-quality data and a lack of research attention and capacity. Hence, there are far fewer climate analyses for these regions, especially in relation to variability and extremes. Impact analyses show that such variability and

* Current affiliation: South African Weather Service, Pretoria, South Africa.

Corresponding author address: Mxolisi E. Shongwe, KNMI, P.O. Box 201, De Bilt, 3730 AE, Netherlands.
E-mail: me_shongwe@yahoo.com

DOI: 10.1175/2010JCLI2883.1

extremes disproportionally affect the poorest countries and the poorest people (e.g., United Nations Poverty–Environment Initiative 2003).

Trying to address that gap, Shongwe et al. (2009, hereafter referred to as Part I) presents an analysis of projected precipitation changes for southern Africa. In this paper, a similar approach is applied to East Africa (EAF), defined as the area of 10°S–4°N, 28°–42°E. The region experiences a semiannual rainfall cycle with two major rainfall peaks in boreal spring [March–May (MAM), also known as long rains] and autumn [September–December (SOND), also known as the short rains]. During the latter season (short rains), atmospheric dynamics in the first month (September) differ from the rest of the season [October–December (OND)]. Also, teleconnections with large-scale features such as the El-Niño–Southern-Oscillation (ENSO) are different between September and OND (Mutai and Ward 2000). It is common practice therefore to omit September when referring to the short rains in East Africa (e.g., Clark et al. 2003; Anyah and Semazzi 2007). We adopt the same convention in this paper. Some portion of the selected area has one rainfall maximum during boreal winter–spring months (November–April).

Traditionally, climate change studies in which Africa is featured have tended to focus on likely precipitation changes during boreal summer and winter (Solomon et al. 2007). Much less is known about the transition seasons (i.e., boreal autumn and spring), which are the rainy seasons in East Africa. Furthermore, there has been a tendency to focus on large regions within Africa or in some cases on the Giorgi regions (Giorgi and Francisco 2000). While this approach is useful in diagnosing the climate change signal on rainfall as a first step, it tends to overlook the effect of local features such as East Africa's varied topography (e.g., mountain ranges and rift valleys) and large water bodies (e.g., Lake Victoria) on the large-scale signal. Although most of these local controls are not yet adequately represented in low-resolution climate models such as those used here, the homogenous subregions identified by Indeje et al. (2000) are used to show that rainfall response to global warming is not uniform across the region.

In recent years, East Africa has suffered frequent episodes of both excessive (e.g., Webster et al. 1999; Latif et al. 1999) and deficient rainfall (e.g., Hastenrath et al. 2007). In particular, the frequency of anomalously strong rainfall causing floods has increased. Our analysis of data from the International Emergency Disaster Database (EM-DAT; http://www.em-dat.net/), reveals that there has also been an increase in the number of reported hydrometeorological disasters in the region, from an average of less than 3 events/year in the 1980s, to over 7 events/year in the 1990s, and almost 10 events/year from 2000 to 2006, with a particular increase in floods; from an average of less than one event per year in the 1980s to seven events per year between 2000 and 2006. In the period 2000–06, these hydrometeorological disasters affected on average almost two million people per year. In addition, they have severe impacts on economic performance and poverty alleviation (e.g., Hellmuth et al. 2007).

Furthermore, we note that many of the region's epidemics, which dominate the remainder of the reported disasters in the EM-DAT database, are also affected by climatic conditions. While part of the trend is due to better reporting, it also reflects a rising vulnerability to natural hazards and, potentially, an underlying trend in climate variability and extremes. These rising risks are receiving increasing attention from policy makers, for example, in the Decision and Declaration on Climate Change and Development adopted by the African Union Head of State Summit in January 2007 and in new efforts by East African governments to better manage climate risks. In Kenya for instance, the Kenya Adaptation to Climate Change in Arid Lands (KACCAL) project aims to address the increasing risk of both floods and droughts (World Bank 2006).

In this context, there is an obvious need for better analyses of the likely response of extreme climate events in this region to global warming, to inform disaster preparedness and development planning. Such demands provided the motivation for the present study. The primary aim is to assess how the intensity of seasonal precipitation extremes is likely to change in the region, against the backdrop of probable changes in mean precipitation. A secondary aim is to assess the spatial inhomogeneities in the model projections. We also present physical mechanisms that may explain the simulated changes in the precipitation probability distribution.

2. Data and methods

a. Model simulations and observations

A brief description of the datasets used and the analysis methods applied are given below. Further details can be found in Part I. The models used in the Intergovernmental Panel on Climate Change (IPCC) Fourth Assessment Report (AR4) (Solomon et al. 2007) form the major input to the analysis of changes in precipitation patterns. The output has been made available as part of the World Climate Research Program (WCRP) Coupled Model Intercomparison Project, phase 3 (CMIP3). We have chosen model projections driven by the intermediate Special Report on Emissions Scenarios (SRES)

A1B scenario, a standard emission scenario currently roughly corresponding to observed CO_2 concentrations. In this scenario, there is no drastic reduction of CO_2 emissions up to 2100, when concentrations reach twice their preindustrial levels. After 2100, experiments have been continued with constant CO_2 concentrations at this level.

A subset of 12 coupled general circulation model (CGCM) simulations has been selected from the data available at the time of first submission (January 2008). The selection was based on a pattern comparison of the seasonal cycle in the simulations for the twentieth century (20c3m) with the Climate Research Unit (CRU TS2.1; New et al. 2000) gridded precipitation. The 12 selected CGCMs were among the six best-performing models (as measured by the mean of the monthly correlation coefficient and root-mean-squared difference with the analysis) over at least one of four domains of sub-Saharan Africa: southern Africa, East Africa, North–East Africa, and West Africa. We also demanded that enough data at high CO_2 concentrations was available to be able to compute return levels. Further details of the selection procedure can be found on the Royal Netherlands Meteorological Institute Africa scenarios Worldwide Web site (www.knmi.nl/africa_scenarios) under technical details.

The selected CGCMs, their spatial resolutions, ensemble sizes, and references are given in Table 1 of Part I. The model simulations are linearly interpolated to a common 1.25° × ~1.24° latitude–longitude grid, corresponding roughly to T95 resolution. As in Part I, two subsamples have been selected from the model simulations. The 1901–2000 and 2051–2200 periods define the present (20c3m) and future climate, respectively.

In addition to monthly CMIP3 precipitation, the horizontal wind vector and pressure vertical velocity (ω) fields are used. These variables are used to estimate the strength and structure of the Eastern Hemisphere zonal (Walker) circulation and their projected changes. Three of the models[1] used in the precipitation change analysis have been omitted in the analysis of the zonal circulation. The CGCM background Walker circulation is compared with that obtained from the 40-yr European Centre for Medium-Range Weather Forecasts Re-Analysis (ERA-40) (Uppala et al. 2005).

[1] The ECHO-G model has been omitted because horizontal wind and pressure velocity fields are not available on the IPCC AR4 archive in both their 20c3m and SRES A1B runs. For the CSIRO Mk3.0, the vertical velocity fields are not available. For the third climate configuration of the Met Office Hadley Centre Unified Model (HadCM3), SRES A1B horizontal wind and vertical velocity fields are not available.

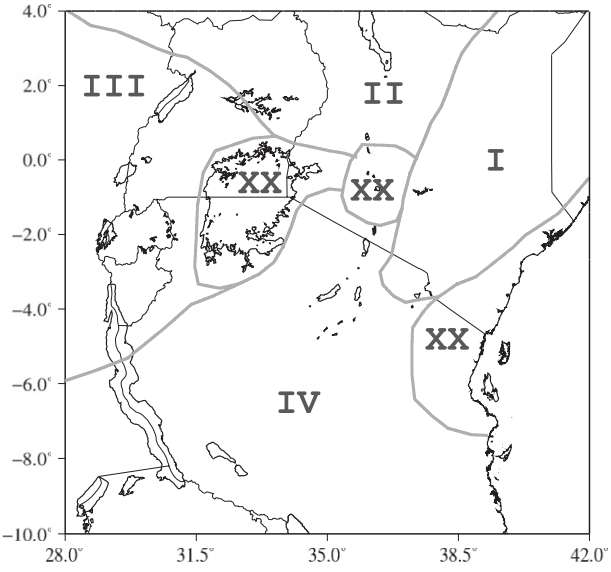

FIG. 1. Location map of the East Africa climatic zones adopted from Indeje et al. (2000). Region III on the west is a combination of two of the Indeje et al. (2000) original zones. Regions that are not large enough to be adequately resolved by the lowest-resolution AR4 CGCMs (shown by XX) have been omitted in our analyses.

Observed twentieth-century precipitation used in this study was taken from the CRU TS2.1 gridded station data. Unlike in Part I, a dearth of station observations in the Global Historical Climatology Network (GHCN) data precluded delineating homogenous rainfall zones. For this reason, the climate zones defined by Indeje et al. (2000) have been adopted in this study. These zones are shown in Fig. 1. The western zones of Indeje et al. are combined into one zone (Zone III, Fig. 1) to allow a larger spatial sampling. In most models used here, precipitation in these areas have similar probability density functions (PDFs, not shown). The CRU TS2.1 grid points falling within each zone are averaged. All the zones except much of Tanzania (Zone IV) have a semiannual cycle. In Zone IV, the annual cycle of area-averaged precipitation showed a peak during austral summer–autumn months (November–April). The CMIP3 simulated precipitation is spatially averaged analogous to the CRU TS2.1 data. The coastal region, the central region of Kenya, and the Lake Victoria area are small enough to be adequately resolved by some low-resolution CGCMs. These regions have therefore been omitted in the analysis.

Monthly precipitation from the CRU TS2.1 gridded station and CMIP3 data are accumulated into seasonal totals for each rainfall season of East Africa. Mean precipitation rates (mm day^{-1}) in a given season are calculated by dividing the seasonal totals by the number of

days within that season. Climatologically wettest seasons are defined as those with the highest mean precipitation rates. On the other hand, the driest seasons, characterizing meteorological droughts, have the lowest mean precipitation rates.

b. Extreme value analysis

The peak over threshold or generalized Pareto distribution (GPD) is used in this study to represent the distribution of observed and simulated extreme seasonal precipitation rates. A description of GPD and its applications is found in Coles (2001). The quality of the GPD fit is then assessed using Anderson–Darling goodness-of-fit tests (Laio 2004). Details of how the GPD has been applied in our work, including statistical tests, are discussed in Part I.

Return levels are estimated from the fitted GPD. Return levels are frequently used in extreme precipitation studies in climate research (e.g., Kharin and Zwiers 2000; Meehl et al. 2005; Kharin et al. 2007) because of the simplicity of their interpretation. The return level (z_p) is the threshold likely to be exceeded in a given year with probability p, or the level likely to be exceeded once in every $1/p$ years. In this study 10-, 20-, 50-, and 100-yr return levels have been estimated. The return values are computed for each homogenous zone (Fig. 1) in both OND and MAM seasons. Owing to the small sample size of threshold excesses, only results based on the least biased 10-yr return levels are presented in this paper. These GPD quantiles (10-yr return levels) are obtained from an interpolation rather than an extrapolation. Results obtained using 100-yr return levels are available on the KNMI Africa scenarios Worldwide Web site (http://www.knmi.nl/africa_scenarios/).

When modeling dry extremes following the approach discussed in Part I, a problem is encountered during extrapolation to much longer return periods because these extremes are by definition constrained by zero above (i.e., dry extremes have a finite upper bound). In practice, almost all GPD fits used in this study have a negative shape parameter ξ and the resulting finite return level for infinite return times are, in fact, positive. The finite upper bound of dry extremes is therefore not a concern in this study.

c. Multimodel ensembling

Uncertainties are inherent in long-term climate model simulations. These can be attributed to natural climate variability, different model responses to a given forcing (such as increases in greenhouse gas concentration), and those associated with the emission scenarios used to force the climate models. In climate change studies devoted to precipitation extremes and their possible future changes, it has become common practice to use simulations from a range of climate models (e.g., Kharin et al. 2007). Research on how best to combine simulations from several climate models through objective weighting is ongoing (e.g., Giorgi and Mearns 2002, 2003; Tebaldi et al. 2004, 2005).

Using the Bayes theorem and making certain assumptions, it is possible to objectively assign weights to different climate models leading to a probability distribution of future climate change. These assumptions detailed by Tebaldi et al. (2005) relate to model bias, model independence, and the similarity of physical mechanisms determining the unforced and future climate. This method has been adopted in the present study. We note here that equal weighting of the models yields similar mean results to the Bayesian weighing method used to obtain the results presented in section 3. However, the credibility intervals obtained by the Bayesian method are smaller due to, among other things, downweighting obvious outliers. It should be noted that there is the possibility that this makes the method overconfident.

For comprehensive details of this method, the reader is referred to Tebaldi et al. (2005). The Bayesian method requires that the input variables have Gaussian likelihoods. Mean precipitation taken over sufficiently long periods (100 or 150 years in this study) meet this requirement from the central limit theorem. To fulfill this requirement in the case of extreme quantiles, the first step involved estimating the GPD parameters from maximum likelihood. After checking for model quality and inverting the GPD to obtain the 10-yr return levels, we then use the delta method described by Coles (2001) to estimate the uncertainty on the return levels. We verified that the 95% credibility interval obtained using this method is very similar to the interval computed with a nonparametric bootstrap method. More details of the methodology used to obtain the GPD quantiles can be found in appendix A of Part I.

To summarize, in the Bayesian framework used, the ratio of the conditional posterior mean of future climate (ν) to control climate (μ) simulations is used to define the relative precipitation change (ΔP) as

$$\Delta P = 100\left(\frac{\nu}{\mu} - 1\right). \quad (1)$$

For mean precipitation rates and 10-yr wettest events, $\Delta P > 0$ is indicative of an increase in their intensity. An increase in the severity of 10-yr driest events is indicated by $\Delta P < 0$. As previously mentioned, these changes compare statistics computed using data for the 1901–2000 (present) period with their counterparts in the 2051–2200 (future) period.

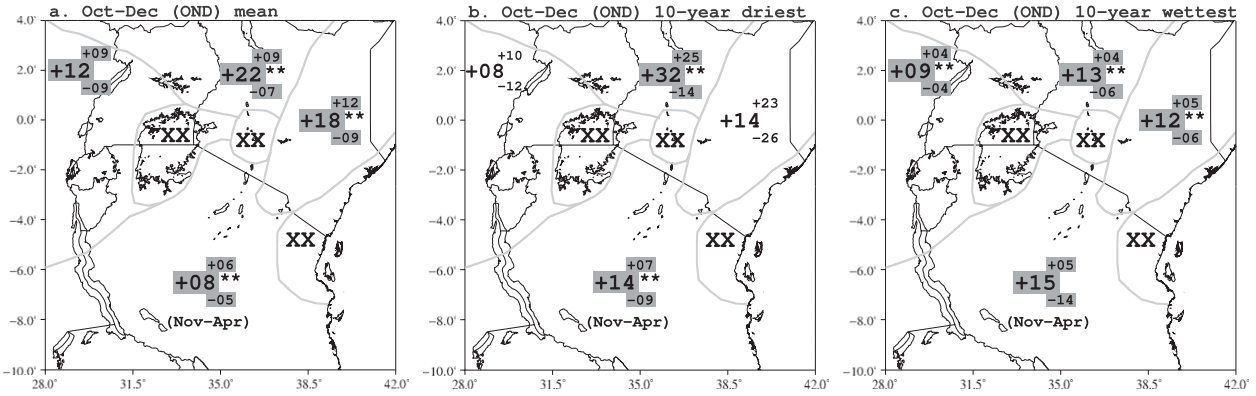

FIG. 2. Projected changes (%) in OND (short rains) (a) mean precipitation rates, (b) 10-year driest events, and (c) 10-year wettest events in each climatic zone. In much of Tanzania (Zone IV, Fig. 1) the displayed precipitation changes are for the austral summer–autumn (November–April) season. In each case, three values are plotted. The middle number gives the mean projected change preceded by its sign (positive for increase and negative for decrease). The number above (below) the mean change, preceded by a positive (negative) sign gives the distance to the upper (lower) critical value of the 95% credibility interval. Projected changes that exclude zero from the 95% (99%) credibility interval are shaded in gray (shown by two asterisks).

3. Changes in mean and extreme precipitation

The Bayesian method adopted in this study enables an estimation of the posterior distribution of the parameters of interest (Tebaldi et al. 2005). The uncertainties associated with these parameters are then inferred from their posteriors. It should be kept in mind that these depend on the prior and the availability of GCM data and, as such, only give an indication of the uncertainties in the return levels. In the following subsections, we present the 95% credibility interval of ΔP as obtained from the Bayesian method for each zone and rainy season of East Africa. We present the results on maps to allow a concise visual interpretation and an easy assessment of the spatial pattern of the projected changes. When the 95% credibility interval shown in the maps excludes zero (i.e., no change), the percentage changes are shaded gray. When zero is outside the 99% credibility interval of ΔP, this is denoted by two asterisks.

a. Short-rains season (October–December)

Mean OND precipitation increases are simulated almost everywhere in East Africa (Fig. 2a). Over the semiarid areas in northern Kenya (Zones I and II; Fig. 1), in the western parts, which include Rwanda and Burundi (Zone III), mean precipitation is projected to increase by more than ~10%. These increases, thus achieved, exclude zero from the 95% credibility interval almost everywhere, and zero is excluded from the 99% credibility interval to the north. Over much of Tanzania (Zone IV), the model projections provide evidence in support of an increase in precipitation rates during austral summer–autumn months (November–April). While most models show an increase in mean OND precipitation, the Hadley Centre Global Environmental Model version 1 (HadGEM1) model shows decreases in rainfall almost everywhere in the area. The convergence criterion used in the Bayesian weighting (Tebaldi et al. 2005) treats this model as an outlier and down weighs it.

A reduction of the severity of the 10-yr driest seasons is found over almost the entire East African region (Fig. 2b). The magnitudes of the simulated reduction in the severity of these OND dry extremes are comparable with those of the mean precipitation rates. Larger reductions (~32%), are found in northern Kenya and Uganda (Zone II). Elsewhere in the north, the projected lessening of the 10-yr droughts severity is not statistically significant. Austral summer–autumn 10-yr droughts are becoming less severe in much of Tanzania by about 14%.

In common with changes in the mean precipitation rates, widespread increases in the intensity of 10-yr wettest OND seasons are simulated (Fig. 2c). Significant increases exceeding ≥10% are found in Kenya, Uganda, and the western parts. In northeastern Democratic Republic of Congo (DRC) and much of Tanzania (Zone IV), increases in the 10-yr wettest austral summer seasons average ~15%.

b. Long-rains season (March–May)

Changes in mean precipitation during the long-rains season (MAM) have generally the same sign and magnitudes as those simulated for the short rains (Fig. 3a). The Bayesian weighted model simulations project more than ~15% increase in mean precipitation rates over much of East Africa. The upper credibility limit exceeds ~25% over a large area to the north and west. However,

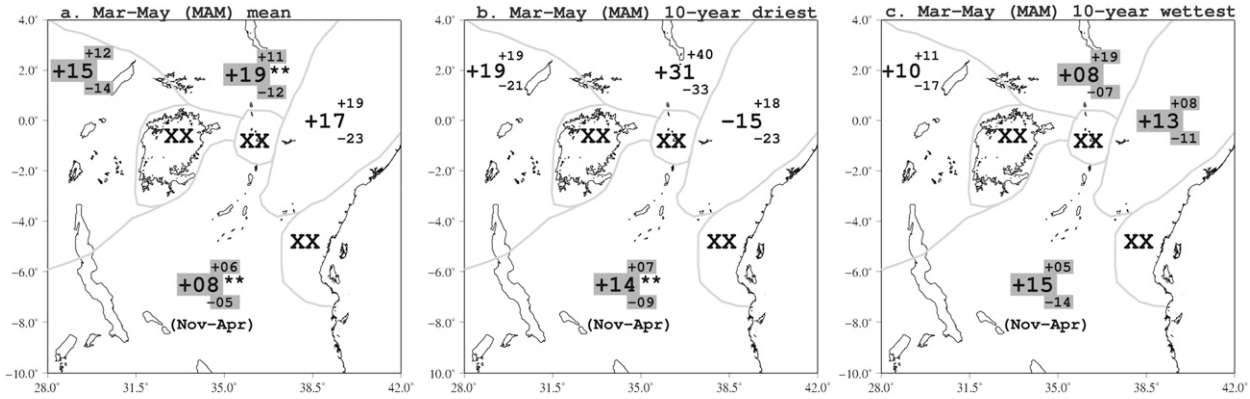

FIG. 3. As in Fig. 2 but for the March–May (long rains) season.

in contrast to the short rains, the models perform poorly in simulating the twentieth-century climate during this season. During the model preselection process, relative to the OND season, correlation between the monthly CRU and model-simulated MAM precipitation was found to be low while the rms error (RMSE) scores were found to be higher (not shown). The difficulty in modeling precipitation during the long rains has been found in seasonal climate predictability studies and is due to a dominance of internal atmospheric variations (not probably connected to other components of the climate system; Mutai et al. 1998). The uncertainty associated with these patterns is higher than in the short-rains season. The models show a reduction in the severity of 10-yr droughts almost everywhere except over eastern Kenya (Fig. 3b). In eastern Kenya, where changes in dry and wet extremes have opposite signs, an increase in interannual rainfall variance is implied. Changes in the 10-yr wettest seasons are of the same sign as those of mean precipitation rates, implying that floods are likely to become more intense (Fig. 3c). However, we place less emphasis on these projections owing to their lower reliability. Again, the HadGEM1 simulations that simulate a drying trend everywhere has been downweighted by the convergence criterion.

c. *Time-series analysis*

Time-series plots for East Africa precipitation during the twentieth (observed and simulated) and twenty-first centuries (simulated) and in each rainy season are shown in Fig. 4. Unlike in Figs. 2 and 3, where the CGCMs are subjected to a Bayesian weighting, the models are equally weighted in these plots. Despite the wider intermodel dispersion in their twenty-first-century projections [caused mainly by the outlying HadGEM1 (dry) and the Model for Interdisciplinary Research on Climate 3.2 (MIROC3.2) (wet) CGCMs], there is substantial evidence in support of an increase in the amount of rainfall. The sharp precipitation increase in East Africa emerges from the early part of the twenty-first century and in most cases is a reversal of drier conditions experienced during much of the last century. We note however that in some regions (e.g., Burundi, Rwanda, and Tanzania; Figs. 4c,d), the observed trend over the last decades of the twentieth century is opposite the long-term CGCMs simulated trend. This can be due to decadal variability that happens to be opposed to the long-term trend in the models or due to the CGCM deficiencies in the small regions considered in our study. Further modeling work to distinguish between these possibilities is required.

A trend toward predominantly positive precipitation anomalies is also present in the long-rains twenty-first century time series (Figs. 4e–f). However, the signal-to-noise ratio in these projections is low.

Noteworthy, the results from the Bayesian weighted and unweighted simulations are broadly similar. By downweighing outlying CGCMs, the Bayesian procedure offered the additional value of reducing the model dispersion by about a factor of 2, particularly in the twenty-second-century simulations when the model spread is largest.

4. Projected changes in large-scale forcing

The robust climate change signal in East Africa precipitation presented above prompts us to endeavour to diagnose likely physical mechanisms and forcings. There is considerable consensus between observational, theoretical, and modeling studies with regard to an increase in vertically integrated atmospheric water vapor as the climate warms (Zveryaev and Chu 2003; Trenberth et al. 2005; Zveryaev and Allan 2005). Related to this is a robust projection of precipitation increase in the deep tropics, which has been detected in the current climate (Zhang et al. 2007). The zonal mean precipitation in the tropics increases because the 7% $°C^{-1}$ increase in

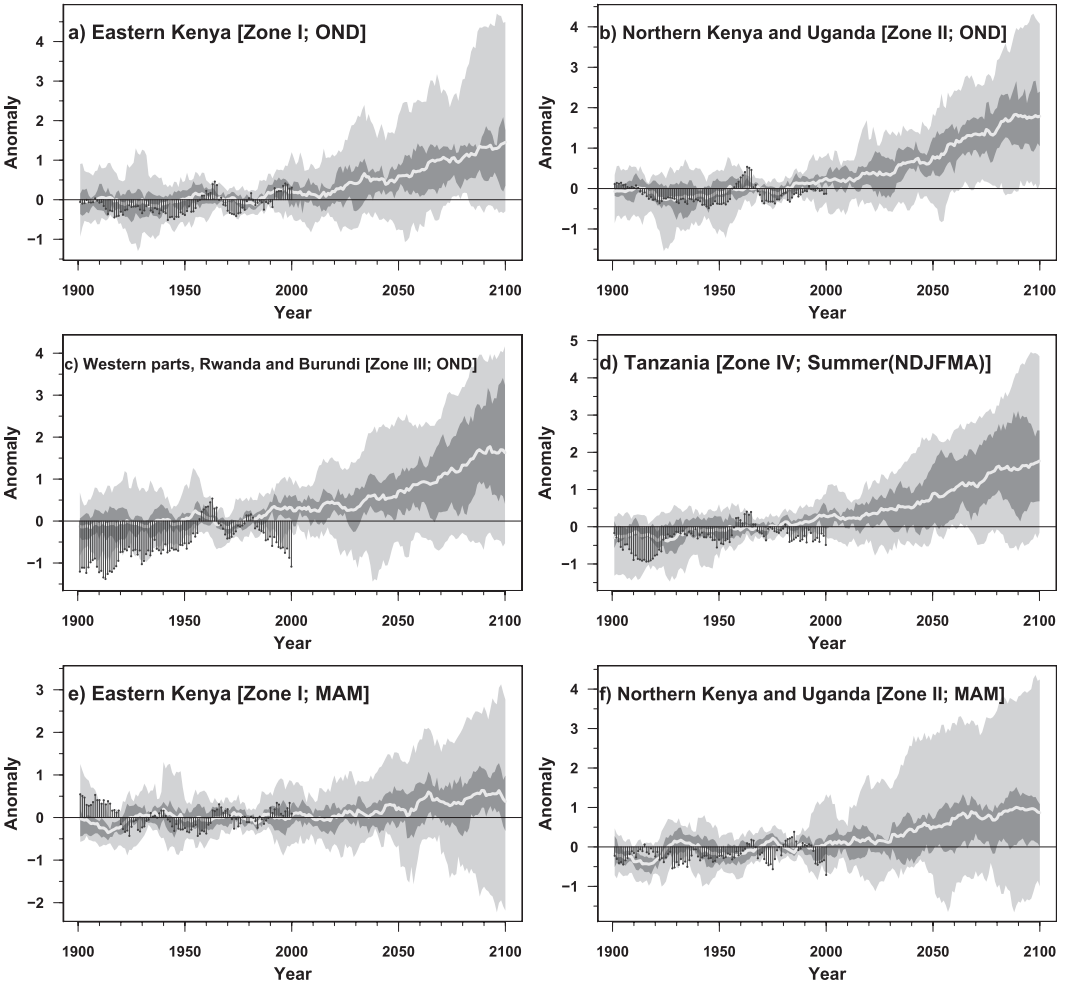

FIG. 4. Time series of observed and simulated precipitation anomalies (std dev, σ) with reference to the 1961–90 climatology: (a)–(c) time series for OND rainfall; (d) the series for much of Tanzania (Zone IV, Fig. 1) during austral summer–autumn (November–April; NDJFMA); the series for MAM precipitation in (e) eastern Kenya (Zone I) and (f) northern Kenya and Uganda (Zone II). The black vertical lines terminated by circles display the observed twentieth-century precipitation from CRU data. The white line shows the ensemble average; the darker and lighter gray shadings indicate 50% ($[q_{0.25}, q_{0.75}]$) and 95% ($[q_{0.025}, q_{0.975}]$) of the distribution, respectively.

precipitable water, which follows the Clausius–Clapeyron relationship, is not completely compensated by a slowdown of the tropical circulation (Held and Soden 2006; Vecchi and Soden 2007).

The increase in precipitation in the tropics is not zonally uniform, with East Africa precipitation projected to increase more than the zonal mean in the multimodel mean. These zonal asymmetries in tropical precipitation response to global warming suggest that other mechanisms also exert a significant influence. These partly stem from the atmospheric dynamic response, which is not zonally symmetric and leads to a horizontal redistribution of water vapor.

To understand this we turn to the well-understood interannual variability in the region. Our hypothesis is that the climate change signal will be communicated to the rainfall field partly through the same factors that control interannual rainfall variability in the present climate. At interannual time scales, Hastenrath et al. (1993) discussed atmospheric forcing on the Indian Ocean hydrosphere. A number of papers documenting atmosphere–ocean coupling have appeared in literature (e.g., Webster et al. 1999; Saji et al. 1999; Goddard and Graham 1999). It has been found that atmospheric anomalies of pressure and wind typically precede sea surface temperature (SST) anomalies (Hastenrath and Polzin 2005). Subsequent SST anomalies, in part forced by wind stress anomalies, feed back to the atmosphere, further reinforcing atmospheric anomalies (Goddard and Graham 1999), which often result in precipitation

anomalies. Against this background, modeled changes in SST and atmospheric circulation during the short-rains season are examined in this section.

a. *Projected OND Indian Ocean SST pattern and rainfall relationship*

Observational and modeling studies have linked East African high-frequency rainfall variability during boreal autumn to SST anomalies (Goddard and Graham 1999; Black et al. 2003). Earlier studies aimed at understanding the link between East Africa precipitation and equatorial Pacific Ocean SSTs associated with ENSO (e.g., Hastenrath et al. 1993; Indeje et al. 2000). It was found that ENSO exerts some influence on East Africa short rains such that rainfall is enhanced (suppressed) during warm (cold) events in the eastern equatorial Pacific Ocean.

It has been shown that the Indian Ocean is one of the pathways through which the ENSO signal propagates into East Africa precipitation. Often, the west Indian Ocean warming lags that of the eastern equatorial Pacific by a few months (Klein et al. 1999). However, evidence has been presented supporting the existence of an Indian Ocean mode of SST variability independent of ENSO (Saji et al. 1999; Webster et al. 1999). In fact OND 1961, one of the wettest in the twentieth century, was not related to ENSO (figure not shown). The models used in this study do not give a robust signal with respect to changes in the mean state of ENSO (not shown). Based on these findings and the fact that changes in ENSO properties are unlikely to exceed natural variability (van Oldenborgh et al. 2005), possible changes in Indian Ocean SST patterns are investigated in this paper. This is motivated by results from studies that found Indian Ocean SST anomalies to be the dominant factor controlling East Africa short rains (Latif et al. 1999; Goddard and Graham 1999; Black et al. 2003; Clark et al. 2003; Behera et al. 2005; Washington and Preston 2006).

In this study, the 1901–2000 CGCM-simulated East Africa short and long rains were subjected to a standard empirical orthogonal function (EOF) analysis (see, e.g., van den Dool 2007). The first EOF is a monopole pattern describing the largest source of interannual variability in this region, particularly during the short rains. The corresponding principal component series are then regressed on simultaneous Indian Ocean SSTs from each model. The regression of the first principal components (PC 1) on Indian Ocean SSTs is displayed in the first and last columns of Fig. 5. Areas with significant regression at the 5% level (from a two-sided local t test) are shaded.

A statistically significant positive link is found with SSTs in the western tropical Indian Ocean (WTIO), west of ~80°E in most models. In some models [e.g., the Commonwealth Scientific and Industrial Research Organisation Mark version 3.0 (CSIRO-Mk3.0), ECHAM5–Max Planck Institute Ocean Model (MPI-OM), Geophysical Fluid Dynamics Laboratory Climate Model version 2.0 (GFDL CM2.0), GFDL-CM2.1, and Meteorological Institute of the University of Bonn, ECHO-G Model (MIUB ECHO-G)] the ocean area with significant positive association with precipitation extends into the Bay of Bengal. Negative regression coefficients are found in the southeastern Indian Ocean off the coast of Sumatra in almost all models. The figures demonstrate that wetter conditions in East Africa in the CGCMs during boreal autumn often occur when SSTs are warmer in the western Indian Ocean and cooler close to the Maritime Continent. These results are broadly similar to previous findings on Indian Ocean–East Africa rainfall relationships in observational and modeling research work (Black et al. 2003; Clark et al. 2003). The major atmospheric response to the anomalous zonal SST gradients relevant for East Africa short rains is a perturbed Indian Ocean Walker cell (Behera et al. 2005). Low-level easterly anomalies south and close to the equator are a prominent feature in this perturbed local Walker circulation. These moisture-laden winds feed the diabatic-heating-induced anomalous convection close to the warm SST anomaly, with the obvious consequence of enhanced precipitation.

There is no similarly significant link between the long rains (MAM) and simultaneous Indian Ocean SSTs in the models (last column of Fig. 5). Even in models that show some association [e.g., Centre National de Recherches Météorologiques Coupled Global Climate Model, version 3 (CNRM-CM3), MIROC3.2, ECHAM5–MPI-OM, MIUB ECHO-G, and GFDL-CM2.0], the remarkable rainfall link to tropical Indian Ocean SST gradients found during the OND season is not present. We do not know of any documented external control (from other components of the climate system) for the long-rains interannual variability. For this reason, our discussion will focus on the SST patterns likely to influence OND rainfall.

Having established the existence of the Indian Ocean SST signal on rainfall, the model-simulated SST differences (2051–2200 minus 1901–2000) are examined. Boreal autumn (OND) Indian Ocean SST differences are displayed in the middle column of Fig. 5. Statistically significant (at the 1% level) basinwide warming is found. Although SSTs warm throughout the tropical Indian Ocean basin, zonal asymmetries in the warming are evident in most models. The western part of the basin is generally projected to warm more than the eastern. These results are in qualitative agreement with Vecchi

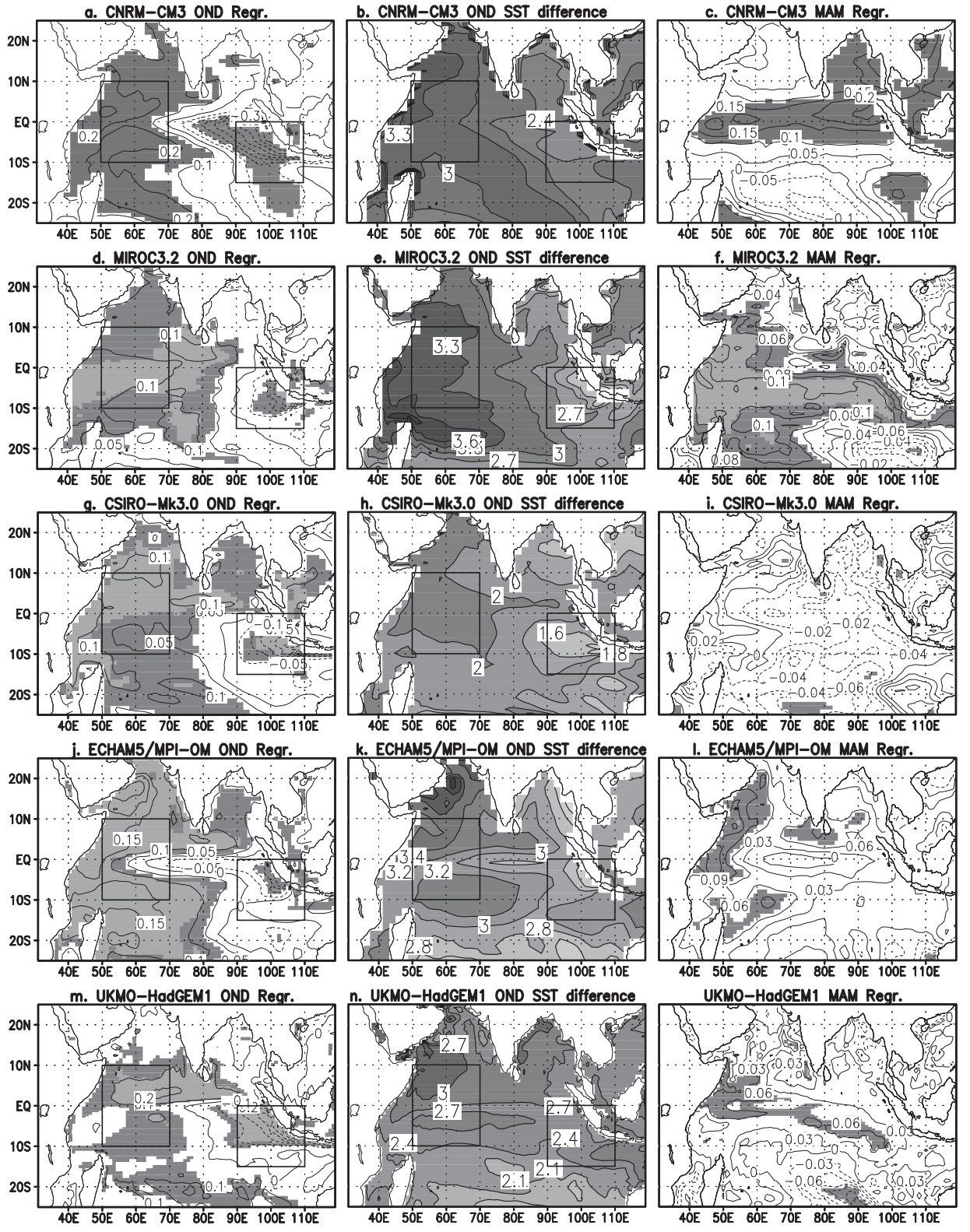

FIG. 5. Regression [positive (solid lines) and negative (dashed lines)] of model-simulated 1901–2000 OND precipitation EOF 1 on simultaneous Indian Ocean SSTs (first column). For each model (name in the title), the second column displays the simulated OND SST difference (°C), that is, 2051–2200 minus 1901–2000. The third column shows the same statistics as column 1, but for the MAM season. In each case, regression coefficients that are statistically significant at the 5% level are shaded gray. Rectangles show areas used to define the Indian Ocean zonal mode index.

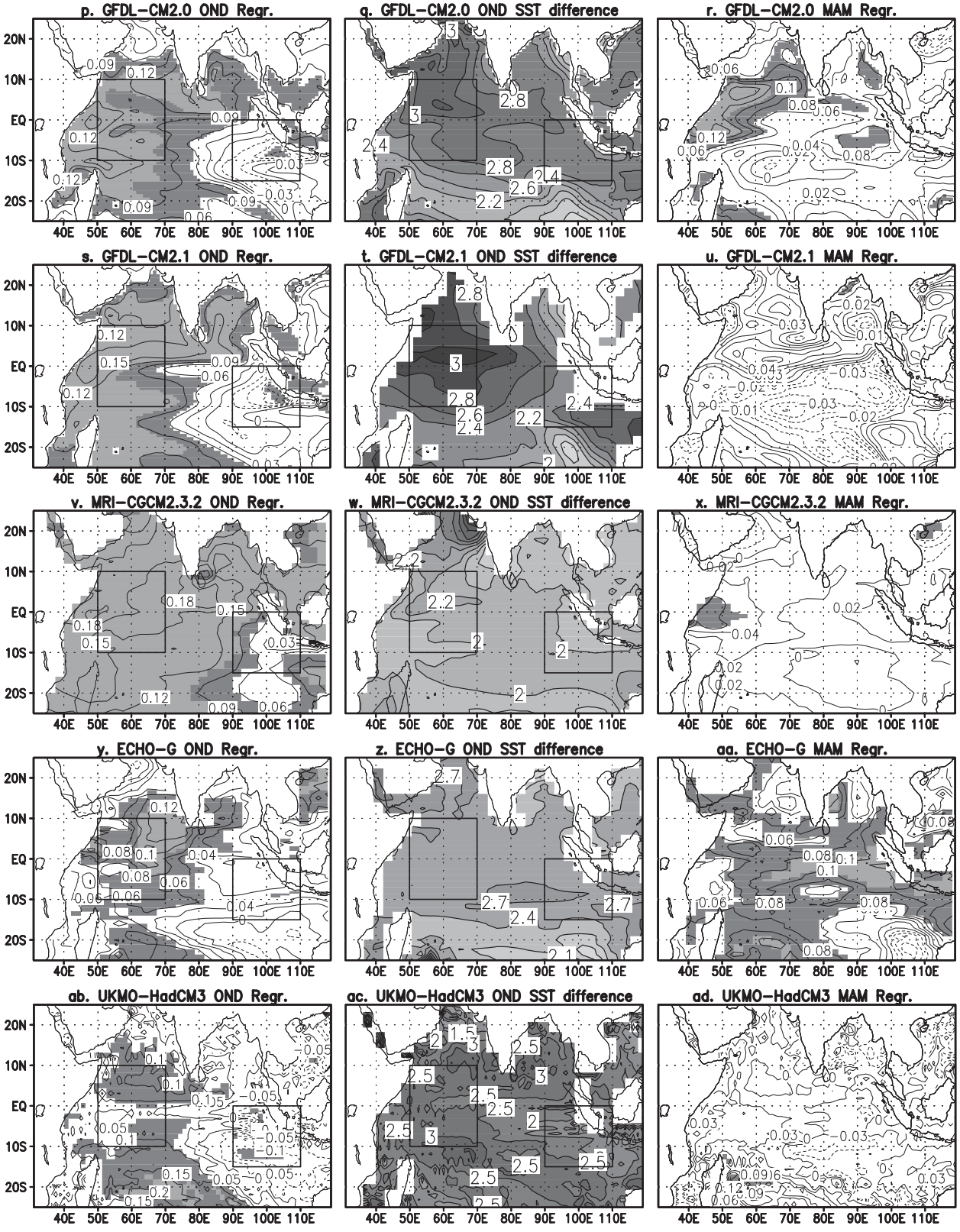

FIG. 5. (*Continued*)

and Soden (2007), who show a tendency toward upwelling (downwelling) along the eastern (western) equatorial Indian Ocean in the twenty-first century (their Fig. 15).

A similar differential warming is observed in interannual variability. It stems from wind–evaporation–SST and wind–thermocline–SST feedbacks which cool the ocean surface in the southeast Indian Ocean (SEIO) from boreal summer to fall before giving way to basinwide warming from around December (Shinoda et al. 2004). Vecchi and Soden (2007) argue that atmospheric anomalies drive changes in tropical ocean dynamics and hence the ocean thermal structure in the twenty-first century. The simulated differential warming and associated anomalous zonal SST gradients have implications for the east–west Indian SST dipole that occasionally peaks during boreal fall months (Behera et al. 2005). As demonstrated above, enhanced rainfall in East Africa is often associated with anomalously warm (cold) SSTs in the WTIO (SEIO).

We proceed by defining an index WTI expressed as average SST in the rectangular domain to the west (10°N–10°S, 50°–70°E) and another index SEI for the box in the eastern extremity (0°–15°S, 90°–100°E). The Indian Ocean zonal mode index (IOZMI), which represents zonal SST gradients across the near-equatorial Indian Ocean, is then defined as IOZMI = WTI–SEI. These boxes are indicated in the first two columns of Fig. 5.

Probability density functions of IOZMI are shown in Fig. 6. Almost all the models displayed in the figure show a clear shift in the PDFs toward a higher probability of positive IOZM phases. This enhanced probability translates to a higher probability of excessive short rains in East Africa in the future climate. These findings are consistent with the results presented in section 3a. On average, the IOZM shift contributes to ~30% [95% confidence interval is (12, 49)] of the overall precipitation change (results not shown).

b. *Changes in Eastern Hemisphere Walker circulation*

In this section, we investigate the circulation changes that give rise to the correlation between the OND Indian Ocean zonal SST gradient and simultaneous precipitation in East Africa. The main changes are in the Walker circulation, which are shown for much of the Eastern Hemisphere stretching from 20°W to 160°E. To define the Walker circulation, we employ the approach used by Chen (2005), and many others, to define atmospheric overturning circulations. In this approach, the first step involves decomposing the horizontal wind vector into its divergent and rotational components. A zonal (meridional) cell is then defined from the zonal (meridional) component of the divergent wind and the vertical velocity.

The tropical zonal circulation plotted in Fig. 7a show three overturning cells. 1) A narrow cell featuring strong ascending motion to the west and subsidence to the east is found in East Africa extending toward the western Indian Ocean. The descending branch of this cell coincides with the semiarid areas in East Africa. The ascending branch corresponds to the major source of diabatic heating over Congo. We refer to this as the East African Walker cell. 2) A shallower East Atlantic cell is found on the west flank of the East African Walker cell. 3) To the east, the East African cell is flanked by a broader Indian Ocean cell. In most models used here, the background zonal circulation is broadly similar to that found in the ERA-40 reanalysis despite the differences in the analysis period considered [1901–2000 and 1958–2000 for the Program for Climate Model Diagnosis and Intercomparison (PCMDI) and ERA-40 data, respectively].

A dominant feature in projected changes in atmospheric upward vertical velocity is a weakening of the ascending branch of the East Atlantic Walker cell over central Africa. A reduction in ω exceeding 2×10^{-4} hPa s^{-1} is found in most models in the middle to upper troposphere. Almost all of the CGCMs show positive differences in the omega velocities over the descending branch of the narrow East African Walker cell. Although not statistically significant in some of the models, these changes imply a weakening of the climatological subsidence over the eastern semiarid regions. These results are in qualitative agreement with Vecchi and Soden (2007), who used different metrics to measure the intensity of the zonal circulation than are used here.

The future behavior of the Eastern Hemisphere Walker circulation shows a tendency toward positive IOZM-like state, consistent with the results presented in section 4a, suggesting that the IPCC AR4 models have physical parameterizations of convective processes that respond realistically to the changes in forcings found here. Vecchi and Soden argue that atmospheric thermodynamics are the principal drivers behind the weakening of the Indo-Pacific Walker circulation. Investigating the cause of the weakening is not the objective of the present study. The aim of our analysis has been to diagnose physical factors underlying the modeled precipitation changes.

5. Discussion and conclusions

In this study we investigated possible changes in the intensity of mean and extreme precipitation rates in East Africa from the CMIP3 multimodel dataset. Evidence in support of a future positive shift in the rainfall

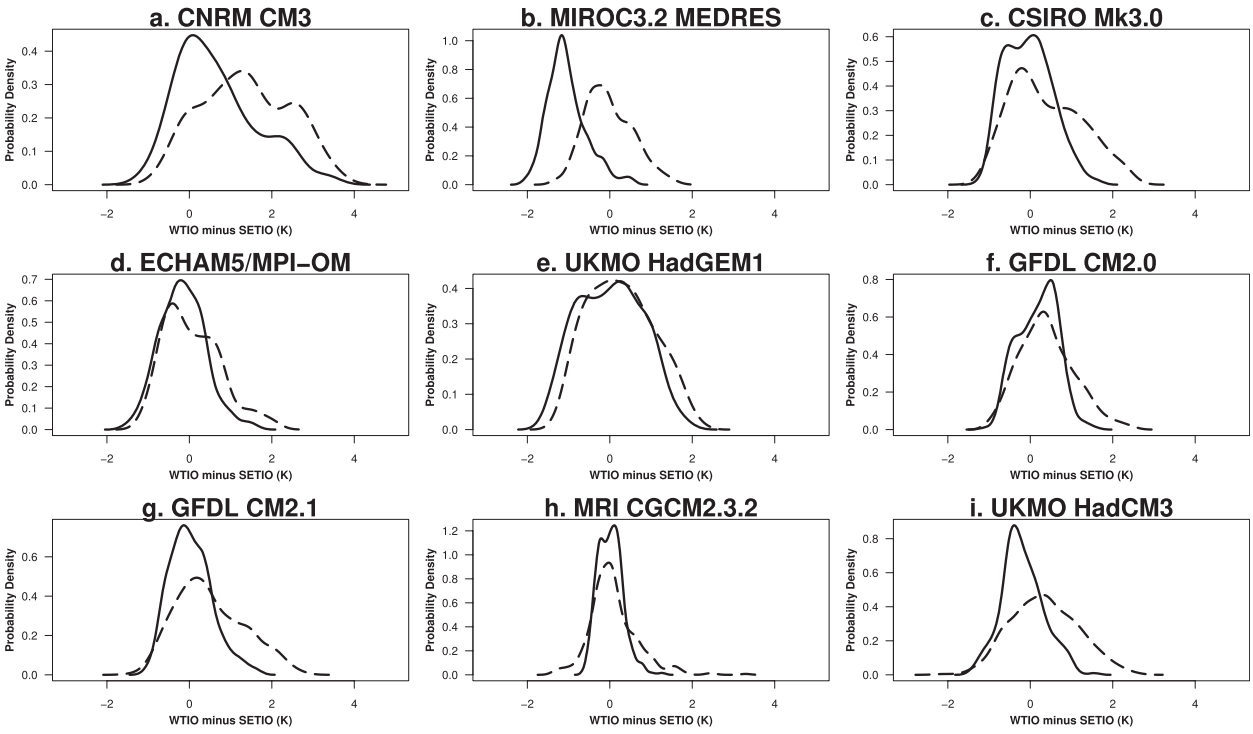

FIG. 6. Probability distribution functions of the IOZM simulated by the selected CGCMs (name given in the title) in the twentieth century (solid line) and future climate (2051–2200; dashed line).

distribution under global warming has been presented for most models, with only a single model simulating a trend to less rain. Increases in both mean precipitation rates and the intensity of 10-yr wettest events are simulated almost throughout the region, while dry extremes are becoming less severe. This is the case even in the semiarid climate in northern Kenya and southern Somalia. The presence of a dipole between southern Africa (cf. Part I) and East Africa in the precipitation response, a robust feature of interannual rainfall variability in the climate system (e.g., Goddard and Graham 1999), is particularly reassuring. A prime example of this feature is the 2006/07 austral summer season. Unprecedented wet conditions in East Africa (Kenya) in November preceded one of the worst droughts in much of southern Africa. The qualitative agreement with previous findings (Kharin and Zwiers 2000; Giorgi and Mearns 2002, 2003; Tebaldi et al. 2004) provides an additional reassurance.

A robust feature across the CGCMs is an increase in atmospheric-column-integrated water vapor during the transition seasons (autumn and spring), particularly in the tropical region. Despite discrepancies in the magnitudes of the linear trends, all models show upward trends in precipitable water in the future climate (not shown). Although the increase in water vapor in a warmer atmosphere is offset to some extent by a slowdown of the tropical circulation (Vecchi and Soden 2007), this trend alone is favorable for an increase in the precipitation almost everywhere in the tropics by about 3% (Held and Soden 2006). Dynamical effects, however, force spatial inhomogeneities in the global-warming-induced tropical rainfall increases. For instance, projections for rainfall in East Africa are higher than the zonal mean. This is in part caused by anomalous moisture flux convergence over East Africa (discussed on the KNMI Africa scenarios Worldwide Web site).

Most models show a stronger boreal autumn warming in the western tropical Indian Ocean relative to the southeastern part of the ocean. This is favorable for a higher probability of positive IOZM events. An important attribute of the positive phase of the IOZM is that it forces excessive short rains in East Africa. It is physically reasonable, therefore, to conclude from this ocean–atmosphere coupling pattern that global warming could enhance the likelihood of anomalously strong short rains. In most subregions of East Africa, dynamically driven rainfall increases, which contribute up to about 30%, are likely to work in concert with other mechanisms to force an overall increase in mean precipitation.

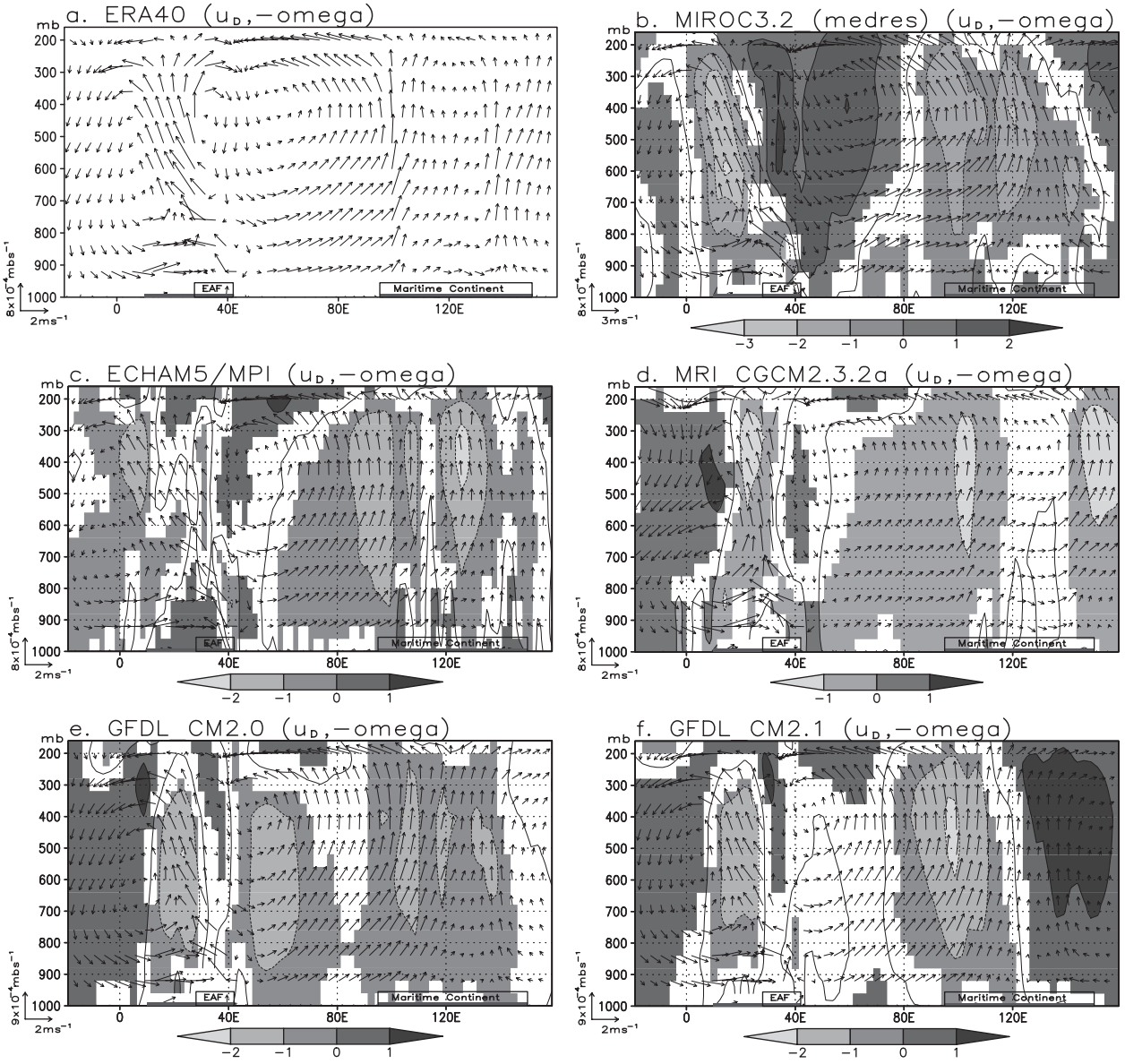

FIG. 7. OND meridionally averaged (10°S–4°N) divergent zonal wind u_D (m s^{-1}) and negatively transformed pressure vertical velocity ω (hPa s^{-1}) in the (a) ERA-40 reanalysis 1958–2000 and (b)–(h) selected IPCC AR4 models. The model names are shown in the titles. Future (2051–2200) minus present (1901–2000) differences in $-\omega$ are superimposed, contour interval 1×10^{-4} hPa s^{-1}. Positive (negative) differences are shown by the solid (dashed) lines. Statistically significant differences at the 5% level (from a z test) are shaded (color bar units are $\times 10^{-4}$ hPa s^{-1}). The approximate locations of East Africa and the Maritime Continent are indicated at the bottom of each panel.

Related to changes in the tropical Indian Ocean zonal SST gradients are changes in the structure of the Eastern Hemisphere Walker circulation. Climatological subsidence over East Africa and the neighboring ocean area is projected to weaken. Boreal fall ascent over the Congo Basin is projected to become either shallower or slower. These features resemble a positive IOZM-like state of the Walker cell, which has been found to communicate the IOZM signal to East Africa precipitation. The presence of such a pattern in the future climate suggests that climate change will to a large extent resemble interannual variability in this regard.

The higher frequency of flooding observed in East Africa in recent years could give indications that the CGCM-simulated precipitation responses are already occurring. Although the time series of the simulated precipitation show upward trends from early in the present century, parts of East Africa could still be

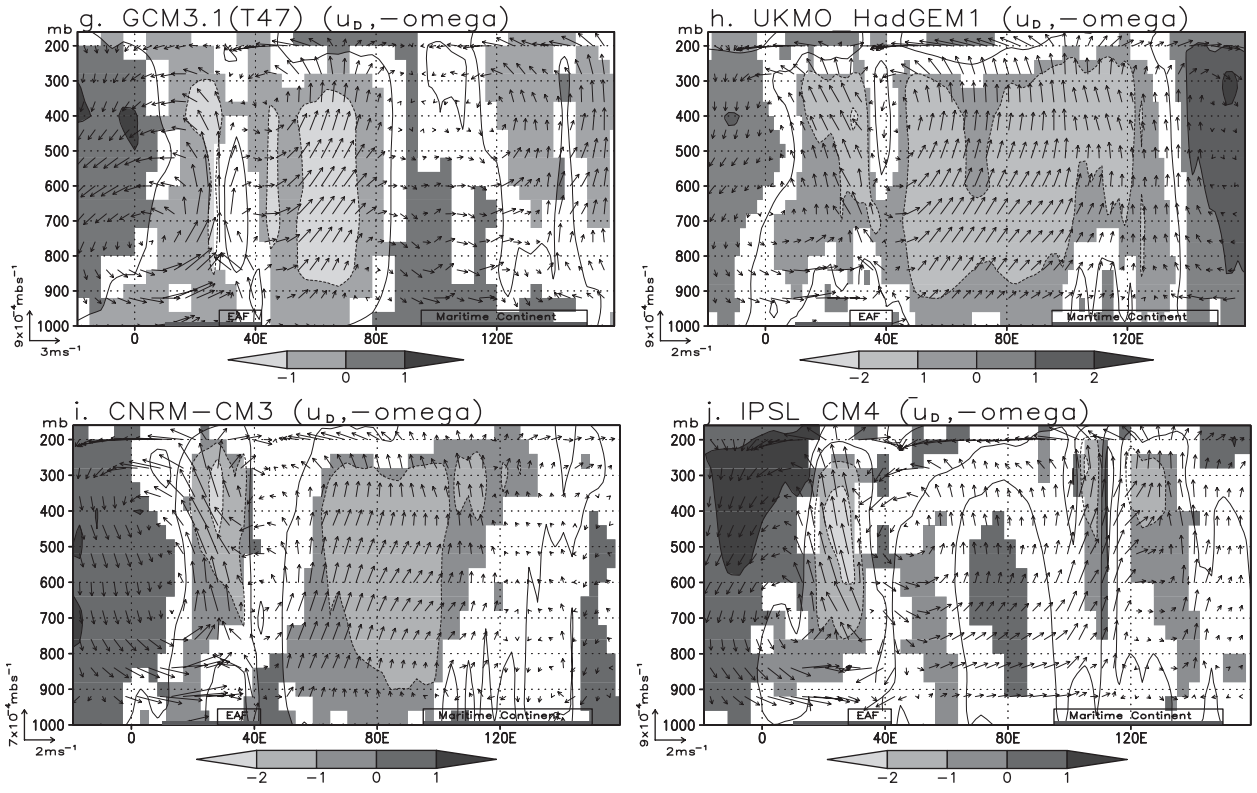

FIG. 7. (*Continued*)

experiencing drier conditions. For example, local trends in Rwanda and Burundi (region III) have been negative over the last decades of the twentieth century, either because of natural variability or model deficiencies in this complex region. From an applications perspective, there have also been reports of continued decline in streamflow and water levels in, for example, Lake Victoria, which may seem paradoxical given the recent high frequency of flooding in East Africa. We note that river/dam levels are also determined by other factors (e.g., water use, drainage, and evaporation), which have not been considered in this paper. Despite the overall positive shift in the rainfall distribution projected in East Africa, the implications of climate change for water resources in this region can only be assessed on the basis of the pattern of precipitation minus evaporation ($P - E$), and its possible spatial and temporal variance, all of which deserve further investigation.

The projected increase in the intensity of 10-yr wettest events translates into rising flood risks for the region, with implications for disaster management, development planning, and local livelihoods. In addition, both the rising temperatures and the higher risk of excessive rainfall have implications for the health sector, for instance, by shifting and/or extending the areas affected by vector-borne diseases such as malaria or the Rift Valley fever.

Acknowledgments. This research has been funded by the Dutch Ministry of Foreign Affairs, Development Cooperation. Claudia Tebaldi provided the MCMC algorithm used in this work. Review comments by Jennifer Barnes, Rein Haarsma, Claudia Tebaldi, the editor, and four anonymous reviewers significantly improved the original manuscript. Technical contributions by Henk van den Brink toward the success of this study are gratefully acknowledged. We acknowledge the modelling groups, the Program for Climate Model Diagnosis and Intercomparison (PCMDI), and the WCRP's Working Group on Coupled Modelling (WGCM) for their roles in making available the WCRP CMIP3 multimodel dataset. Support of this dataset is provided by the Office of Science, U.S. Department of Energy.

REFERENCES

Anyah, R. O., and F. H. M. Semazzi, 2007: Variability of East African rainfall based on multiyear RegCM3 simulations. *Int. J. Climatol.,* **27,** 357–371.

Behera, S. K., J.-J. Luo, S. Masson, P. Delecluse, S. Gualdi, A. Navarra, and T. Yagamata, 2005: Paramount impact of the Indian Ocean dipole on the East African short rains: A CGCM study. *J. Climate,* **18,** 4514–4530.

Beniston, M., and Coauthors, 2007: Future extreme events in European climate: An exploration of regional climate model

projections. *Climate Change,* **81,** 71–95, doi:10.1007/s10584-006-9226-z.

Black, E., J. Slingo, and K. R. Sperber, 2003: An observational study of the relationship between excessively strong short rains in coastal East Africa and Indian Ocean SST. *Mon. Wea. Rev.,* **131,** 74–94.

Chen, T.-C., 2005: Maintenance of the midtropospheric north African summer circulation: Saharan high and African easterly jet. *J. Climate,* **18,** 2943–2962.

Clark, C. O., P. J. Webster, and J. E. Cole, 2003: Interdecadal variability of the relationship between the Indian Ocean zonal mode and East African coastal rainfall anomalies. *J. Climate,* **16,** 548–554.

Coles, S., 2001: *An Introduction to Statistical Modeling of Extreme Values*. Springer, 208 pp.

Gillett, N. P., A. J. Weaver, F. W. Zwiers, and M. D. Flannigan, 2004a: Detecting the effect of human-induced climate change on Canadian forest fires. *Geophys. Res. Lett.,* **31,** L18211, doi:10.1029/2004GL020876.

Giorgi, F., and R. Francisco, 2000: Uncertainties in regional climate change predictions: A regional analysis of ensemble simulations with the HADCM2 GCM. *Climate Dyn.,* **16,** 169–182.

——, and L. O. Mearns, 2002: Calculation of average, uncertainty range, and reliability of regional climate changes from AOGCM simulations via the "Reliability Ensemble Average" (REA) method. *J. Climate,* **15,** 1141–1158.

——, and ——, 2003: Probability of regional climate change based on Reliability Ensemble Average (REA) method. *Geophys. Res. Lett.,* **30,** 1629, doi:10.1029/2003GL017130.

Goddard, L., and N. E. Graham, 1999: The importance of the Indian Ocean for simulating rainfall anomalies over eastern and southern Africa. *J. Geophys. Res.,* **104,** 19 099–19 116.

Hastenrath, S., and D. Polzin, 2005: Mechanisms of climate anomalies in the equatorial Indian Ocean. *J. Geophys. Res.,* **110,** D08113, doi:10.1029/2004JD004981.

——, A. Nicklis, and L. Greischar, 1993: Atmospheric-hydrospheric mechanisms of climate anomalies in the western equatorial Indian Ocean. *J. Geophys. Res.,* **98,** 20 219–20 235.

——, D. Polzin, and C. Mutai, 2007: Diagnosing the 2005 drought in equatorial East Africa. *J. Climate,* **20,** 4628–4637.

Hegerl, G. C., T. R. Karl, M. Allen, N. L. Bindoff, N. Gillett, D. Karoly, X. Zhang, and F. Zwiers, 2006: Climate change detection and attribution: Beyond mean temperature signals. *J. Climate,* **19,** 5058–5077.

Held, I. M., and B. J. Soden, 2006: Robust responses of the hydrological cycle to global warming. *J. Climate,* **19,** 5686–5699.

Hellmuth, M. E., A. Moorhead, M. C. Thomson, and J. Williams, Eds., 2007: *Climate Risk Management in Africa: Learning from Practice*. International Research Institute for Climate and Society (IRI), 116 pp.

Houghton, J. T., Y. Ding, D. J. Griggs, M. Noguer, P. J. van der Linden, X. Dai, K. Maskell, and E. C. A. Johnson, Eds., 2001: *Climate Change 2001: The Scientific Basis*. Cambridge University Press, 881 pp.

Indeje, M., F. H. M. Semazzi, and L. J. Ogallo, 2000: ENSO signals in East African rainfall seasons. *Int. J. Climatol.,* **20,** 19–46.

Karoly, D. J., and K. Braganza, 2005: Attribution of recent temperature changes in the Australian region. *J. Climate,* **18,** 457–464.

Kharin, V. V., and F. W. Zwiers, 2000: Changes in the extremes in an ensemble of transient climate simulations with a coupled atmosphere–ocean GCM. *J. Climate,* **13,** 3760–3788.

——, ——, X. Zhang, and G. C. Hegerl, 2007: Changes in temperature and precipitation extremes in the IPCC ensemble of global coupled model simulations. *J. Climate,* **20,** 1419–1444.

Klein, S. A., B. J. Soden, and N. C. Lau, 1999: Remote sea surface temperature variations during ENSO: Evidence of a tropical atmospheric bridge. *J. Climate,* **12,** 917–932.

Laio, F., 2004: Cramer–von Mises and Anderson–Darling goodness of fit tests for extreme value distributions with unknown parameters. *Water Resour. Res.,* **40,** W09308, doi:10.1029/2004WR003204.

Latif, M., D. Dommenget, M. Dima, and A. Grötzner, 1999: The role of Indian Ocean sea surface temperature in forcing East African rainfall anomalies during December/January 1997/98. *J. Climate,* **12,** 3497–3504.

Meehl, G. A., J. M. Arblaster, and C. Tebaldi, 2005: Understanding future patterns of increased precipitation intensity in climate model simulations. *Geophys. Res. Lett.,* **32,** L18719, doi:10.1029/2005GL023680.

Mutai, C. C., and M. N. Ward, 2000: East African rainfall and the tropical circulation/convection on intraseasonal to interannual timescales. *J. Climate,* **13,** 3915–3939.

——, ——, and A. W. Colman, 1998: Towards the prediction of the East African short rains based on sea surface temperature and atmosphere coupling. *Int. J. Climatol.,* **18,** 975–997.

New, M., M. Hulme, and P. Jones, 2000: Representing twentieth-century space–time climate variability. Part II: Development of 1901–96 monthly grids of terrestrial surface climate. *J. Climate,* **13,** 2217–2238.

Saji, H. N., B. N. Goswami, P. N. Vinayachandran, and T. Yagamata, 1999: A dipole mode in the tropical Indian Ocean. *Nature,* **401,** 360–363.

Shinoda, T., M. A. Alexander, and H. H. Hendon, 2004: Remote response of the Indian Ocean to interannual SST variations in the tropical Pacific. *J. Climate,* **17,** 362–372.

Shongwe, M. E., G. J. van Oldenborgh, B. J. J. M. van den Hurk, B. de Boer, C. A. S. Coelho, and M. K. van Aalst, 2009: Projected changes in mean and extreme precipitation in Africa under global warming. Part I: Southern Africa. *J. Climate,* **22,** 3819–3837.

Solomon, S., D. Qin, M. Manning, M. Marquis, K. Averyt, M. M. B. Tignor, H. L. M. Jr, and E. Z. Chen, Eds., 2007: *Climate Change 2007: The Physical Science Basis*. Cambridge University Press, 996 pp.

Tebaldi, C., L. O. Mearns, D. Nychka, and R. L. Smith, 2004: Regional probabilities of precipitation change: A Bayesian analysis of multimodel simulations. *Geophys. Res. Lett.,* **31,** L24213, doi:10.1029/2004GL021276.

——, R. L. Smith, D. Nychka, and L. O. Mearns, 2005: Quantifying uncertainty in projections of regional climate change: A Bayesian approach to the analysis of multimodel ensembles. *J. Climate,* **18,** 1524–1540.

Trenberth, K. E., J. Fasullo, and L. Smith, 2005: Trends and variability in column integrated atmospheric water vapor. *Climate Dyn.,* **24,** 741–758.

United Nations Poverty–Environment Initiative, 2003: Poverty and climate change: Reducing the vulnerability of the poor through adaptation. UNPEI, 56 pp.

Uppala, S. M., and Coauthors, 2005: The ERA-40 Re-Analysis. *Quart. J. Roy. Meteor. Soc.,* **131,** 2961–3012.

van den Dool, H., 2007: *Empirical Methods in Short-Term Climate Prediction*. Oxford University Press, 215 pp.

van den Hurk, B. J. J. M., and Coauthors, 2006: KNMI climate change scenarios 2006 for the Netherlands. KNMI Tech. Rep.WR-2006-01, 82 pp.

van Oldenborgh, G. J., S. Y. Philip, and M. Collins, 2005: El Niño in a changing climate: A multi-model study. *Ocean Sci.,* **1,** 81–95.

van Ulden, A. P., and G. J. van Oldenborgh, 2006: Large-scale atmospheric circulation biases and changes in global climate model simulations and their importance for climate change in central Europe. *Atmos. Chem. Phys.,* **6,** 863–881.

Vecchi, G. P., and B. J. Soden, 2007: Global warming and the weakening of the tropical circulation. *J. Climate,* **20,** 4316–4340.

Washington, R., and A. Preston, 2006: Extreme wet years over southern Africa: Role of Indian Ocean sea surface temperatures. *J. Geophys. Res.,* **111,** D15104, doi:10.1029/2005JD006724.

Webster, P. J., A. M. Moore, J. P. Loschnigg, and R. R. Leben, 1999: Coupled ocean–atmosphere dynamics in the Indian Ocean during 1997–98. *Nature,* **401,** 356–360.

World Bank, 2006: Kenya Adaptation to Climate Change in Arid Lands (KACCAL), GEF project brief. World Bank Rep. 54740, 30 pp.

Zhang, X., F. W. Zwiers, G. C. Hegerl, F. H. Lambert, N. P. Gillett, S. Solomon, P. A. Stott, and T. Nozawa, 2007: Detection of human influence on twentieth-century precipitation trends. *Nature,* **448,** 461–465, doi:10.1038/nature06025.

Zveryaev, I. I., and P.-S. Chu, 2003: Recent climate changes in precipitable water in the global tropics as revealed in National Centers for Environmental Prediction/National Center for Atmospheric Research reanalysis. *J. Geophys. Res.,* **108,** 4311, doi:10.1029/2002JD002476.

——, and R. P. Allan, 2005: Water vapor variability in the tropics and its links to dynamics and precipitation. *J. Geophys. Res.,* **110,** D21112, doi:10.1029/2005JD006033.